Research Article Vol. 8, No. 11 / November 2021 / Optica 1495

OPTICA

Low-threshold InP quantum dot and InGaP quantum well visible lasers on silicon (001)

Pankul Dhingra,[1,2] Patrick Su,[1,2] Brian D. Li,[1,2] Ryan D. Hool,[2,3] Aaron J. Muhowski,[4] Mijung Kim,[1,2] Daniel Wasserman,[4] John Dallesasse,[1,2] and Minjoo Larry Lee[1,2,*]

[1]Department of Electrical and Computer Engineering, University of Illinois Urbana-Champaign, 306 N Wright Street, Urbana, Illinois 61801, USA
[2]Holonyak Micro and Nanotechnology Laboratory, University of Illinois Urbana-Champaign, 208 N Wright Street, Urbana, Illinois 61801, USA
[3]Department of Materials Science and Engineering, University of Illinois Urbana-Champaign, 1304 W Green Street, Urbana, Illinois 61801, USA
[4]Department of Electrical and Computer Engineering, University of Texas at Austin, 2501 Speedway, Austin, Texas 78712, USA
*Corresponding author: mllee@illinois.edu

Received 23 September 2021; revised 20 October 2021; accepted 22 October 2021 (Doc. ID 443979); published 17 November 2021

Monolithically combining silicon nitride (SiN_x) photonics technology with III-V active devices could open a broad range of on-chip applications spanning a wide wavelength range of ∼400−4000 nm. With the development of nitride, arsenide, and antimonide lasers based on quantum well (QW) and quantum dot (QD) active regions, the wavelength palette of integrated III-V lasers on Si currently spans 400 nm to 11 μm, with a crucial gap in the red-wavelength regime of 630–750 nm. Here, we demonstrate red $In_{0.6}Ga_{0.4}$ P QW and far-red InP QD lasers monolithically grown on CMOS-compatible Si (001) substrates with continuous-wave operation at room temperature. A low-threshold current density of 550 A/cm^2 and 690 A/cm^2 with emission at 680–730 nm was achieved for QW and QD lasers on Si, respectively. This work represents a step toward the integration of visible red lasers on Si, allowing the utilization of integrated photonics for applications including biophotonic sensing, quantum computing, and near-eye displays.

https://doi.org/10.1364/OPTICA.443979

The primary application for Si photonics technology to date has been integrated photonic transceivers for telecommunications where off-chip or hybrid-integrated InP-based lasers emitting in the C- or O-bands (∼1.3−1.6 μm) serve as the light source [1]. Leveraging the CMOS foundry, Si photonics now enables an increasing number of applications, including mapping and navigation [2], spectroscopy [3], and quantum communication [4]. Applications that rely on visible lasers, such as biosensing [5], atomic clocks [6], and spatial mapping [2] could greatly benefit from the ability to generate, guide, and sense light on a chip [7]. As another example, integrated photonics could help overcome the limitations of free-space optics for trapped-ion quantum computing relying on 674 nm lasers to drive transitions in $^{88}Sr^+$ ion qubits [8]. Low-loss SiN_x waveguide technology [9] is a key enabler for visible photonics chips, but efforts to integrate visible sources on Si are currently lagging behind.

Despite elevated threading dislocation density (TDD) values of $\sim 10^6-10^8$ cm^{-2} [10], recent efforts have yielded a wide range of monolithic lasers on Si utilizing GaAs-, InP-, and GaSb-based active regions. For example, InAs quantum dot (QD) lasers on GaAs/Si (001) emitting at 1.3 μm, have been demonstrated with threshold current density (J_{th}) values as low as 62.5 A/cm^2 for room temperature (RT), continuous-wave (CW) operation [11]; $J_{th} = 100-300$ A/cm^2 is more typical for InAs QD lasers on Si [12,13]. In addition, Shang *et al.* demonstrated an extrapolated operation lifetime of 22 years with a constant current stress at 80°C by preventing the formation of misfit dislocations in the InAs QD active region [12–14]. As another example, InGaAsP multiple quantum well (MQW) lasers on InP/Si (001) emitting at 1.55 μm with CW, RT operation and $J_{th} = 1-3$ kA/cm^2 have also been reported [15,16]. Finally, GaSb-based quantum well (QW) lasers emitting at 2.3 μm were recently demonstrated using on-axis Si substrates with $J_{th} = 200-300$ A/cm^2 and CW operation up to 80°C [17,18]; further references on epitaxial III-V lasers on Si can be found in recent review articles [10,19,20]. Despite the impressive development of near- and shortwave-infrared lasers on Si based on both QD and QW active regions, there are no reports for electrically injected red lasers on on-axis Si. Development of monolithic visible red lasers on Si would fill a crucial gap in the wavelength palette of integrated lasers on Si, which already spans 400 nm [21] to 11 μm [22].

$In_xGa_{1-x}P$ QWs and InP QDs are a versatile platform for high-efficiency diode lasers emitting in the 630–800 nm wavelength regime. InP QD lasers on GaAs emitting in the 680–750 nm [23,24] wavelength range have shown pulsed J_{th} values as low as 190 A/cm^2 [24] and high-power output >150 mW [25]. Compressively strained $In_xGa_{1-x}P$ ($x > 0.49$) QW lasers on GaAs are even more mature and have demonstrated watt-class power output [26] with J_{th} of 295 A/cm^2 [27]. Kwon *et al.* demonstrated the first $In_{0.58}Ga_{0.42}P$ QW lasers on 6° offcut Si (001) using a 10-μm-thick SiGe buffer with TDD = 2×10^6 cm^{-2} [28]. Despite the well-controlled TDD, the lasers only operated pulsed

with a high J_{th} of 1.65 kA/cm^2, and moreover, the use of offcut Si substrates renders such devices incompatible with Si photonics foundries [28]. More recently, Luo *et al.* demonstrated optically pumped InP QD microdisk lasers on Si (001) [29]. Despite the excellent performance of phosphide-based visible lasers on GaAs, further work is required to monolithically integrate visible lasers and optical amplifiers on Si (001).

To date, no electrically injected red laser has been demonstrated on exact Si (001), preventing visible integrated photonics from fully leveraging advances in high-performance SiN_x passive optical components and Si photodetectors. In this paper, we demonstrate what we believe are the first visible $In_{0.6}Ga_{0.4}P$ QW and InP QD lasers monolithically grown on foundry-compatible Si (001) substrates with CW, RT operation. Despite a moderate increase in J_{th} caused by threading dislocations, our visible lasers on Si (001) compare favorably with earlier-reported devices based on similar active regions grown on GaAs (001). Low-threshold, monolithically integrated visible lasers on Si can serve as an important low-cost enabler for visible optoelectronics applications ranging from quantum information [4] to near-eye displays [30].

All lasers were grown in a Veeco Mod Gen II solid-source molecular beam epitaxy (MBE) system on GaAs (001) and GaAs/Si (001) without any intentional offcut. We grew relaxed GaAs on GaP/Si (001) templates commercially available from $NAsP_{III-V}$ GmbH using a combination of thermal cycle annealing and dislocation filtering [31] (Supplement 1); the total thickness of the buffer layer was ∼2.15 μm. The laser structure [Fig. 1(a)] includes an optical cavity consisting of 1000 nm n- and p-$Al_{0.51}In_{0.49}P$ (AlInP, hereafter) cladding layers and a 150 nm $(Al_xGa_{1-x})_{0.52}In_{0.48}P(x = 0.34 - 1)$ continuous graded index waveguide (GRIN-WG) layer. We grew $In_{0.48}Ga_{0.52}P$ barrier reduction layers (BRLs) between the GaAs contact and AlInP cladding layers to mitigate voltage drops resulting from band offsets [32]. The cladding, waveguide, and BRLs were lattice-matched to GaAs, as confirmed by high-resolution x-ray diffraction. The active region of the single QW (SQW) laser consists of a compressively strained 7 nm $In_{0.6}Ga_{0.4}P$ QW surrounded by 50 nm, 2.1 eV $Al_{0.17}Ga_{0.35}In_{0.48}P$ (AlGaInP, hereafter) spacer layers, lattice-matched to GaAs. The active region of the InP multiple quantum dot (MQD) lasers utilizes a QD in a well design (QDWELL) with 3.5 monolayers (MLs) InP QDs capped by a 7 nm $In_{0.6}Ga_{0.4}P$ QW and surrounded by 16 nm AlGaInP spacer layers; the QDWELL structure was repeated 3× in the InP MQD laser. The MQD active region was utilized to increase modal overlap with the gain region, consistent with prior reports [23–25]; in contrast, the majority of low-threshold $In_xGa_{1-x}P$ QW lasers utilize an SQW active region [26,27]. All laser structures underwent post-growth rapid thermal annealing (RTA) at 950°C for 1 s to improve the optical quality of the active region [33] prior to fabrication of uncoated, broad-area lasers (Supplement 1). Details of the beneficial effect of RTA on both photoluminescence (PL) and laser threshold characteristics will be discussed in a future publication. Laser testing was performed under CW injection with devices sitting on a temperature-controlled stage (see Supplement 1 for current-voltage curves and other testing details). Reliability studies are planned for the future, but we see no evidence of degradation over the time spent characterizing these devices.

The bright-field transmission electron microscope (BF-TEM) image in Fig. 1(b) shows an entire InP MQD laser structure grown on GaAs/Si. The striated contrast throughout the device is common for ternary and quaternary AlGaInP alloys grown by MBE and results from weak phase separation during growth [34]. The active region shows three layers of coherently strained InP QDs exhibiting a mottled, dark strain contrast, while the apparent absence of threading dislocations indicates that the TDD in the active region is close to or below the detection limit of $\sim 1 \times 10^7$ cm^{-2}. Importantly, no misfit dislocations are observed in the active region, despite the compressive strain present in both the InP QDs and $In_{0.6}Ga_{0.4}P$ QWs. A high-angle annular dark-field scanning TEM (HAADF-STEM) image of a single QDWELL layer in Fig. 1(c) shows the composition contrast of individual InP QDs. The density of buried InP QDs, calculated using BF-TEM is $>1 \times 10^{11}$ cm^{-2}, consistent with our previous report [35]. The panchromatic cathodoluminescence (CL) map in Fig. 1(d) of the n-GaAs/Si virtual substrate used for the laser growth confirms the TDD value of $\sim 1 \times 10^7$ cm^{-2}.

A critical precursor towards demonstrating low-J_{th} red lasers on Si was to develop high-performance benchmark devices on native GaAs substrates, and Fig. 2(a) shows the light intensity versus current density (L-I) characteristics of broad-area $In_{0.6}Ga_{0.4}P$ SQW and InP MQD lasers on GaAs tested under CW operation at 20°C. The $In_{0.6}Ga_{0.4}P$ SQW laser shows a low J_{th} of 170 A/cm^2 with an output power of >10 mW, while the InP MQD laser exhibits a slightly higher J_{th} of 230 A/cm^2 (77 A/cm^2 per QDWELL layer) due to its thicker active region. Although a pulsed J_{th} value of 190 A/cm^2 has been reported previously for InP MQD lasers [24], these are the lowest CW J_{th} values on GaAs (001) that we are aware of. Figure 2(b) shows that the $In_{0.6}Ga_{0.4}P$ SQW laser emits at 691.5 nm and the InP MQD laser emits in the far-red regime at 726.8 nm; both exhibit multiple transverse and longitudinal modes, as expected for broad-area lasers; variation in cavity width over a range of 40–100 μm had no systematic effect on the J_{th} or output power of the lasers described in this paper (Supplement 1). The ultralow CW J_{th} of our $In_{0.6}Ga_{0.4}P$ SQW and InP MQD lasers on GaAs establishes that our material quality is at or near state-of-the-art values and enables us to observe the performance of our lasers on Si without the deleterious point defects that have been reported in MBE-grown phosphides [36].

$In_{0.6}Ga_{0.4}P$ SQW lasers on Si (001) exhibit a CW J_{th} of 550 A/cm^2 [Fig. 3(a)], 3× lower than previously reported pulsed devices on offcut Si [28]. The inset of Fig. 3(a) shows a photograph of the laser (cavity length = 1.25 mm, ridge width = 40 μm) located at the bottom/foreground operating at ∼5 mW output power with the far-field pattern projected onto a wall, ∼50 cm from the device under test; the dark/bright vertical stripes in the far-field result from diffraction effects in the elliptical emission pattern. The SQW laser on Si (001) emits with multiple modes centered at 693.9 nm as shown in Fig. 3(b), slightly redshifted compared to the laser grown on GaAs. The redshift could be attributed to tensile strain arising from the thermal mismatch between III-V layers and Si [37]. Despite a TDD of 1×10^7 cm^{-2}, $In_{0.6}Ga_{0.4}P$ SQW lasers show only a moderate increase of 3.2× in J_{th} compared to SQW lasers on GaAs. Besides the impact of threading dislocations, the shorter cavity length (1.25 versus 1.8 mm) of the SQW laser on Si and the narrower ridge width (40 μm versus 100 μm) could be responsible for the increase in J_{th}. The relatively low J_{th} of our $In_{0.6}Ga_{0.4}P$ SQW lasers on Si is noteworthy, considering that earlier work used GaAs/Si with a much lower TDD of 2×10^6 cm^{-2} [28]. We believe that non radiative recombination at point defects is the most likely reason for the high J_{th}

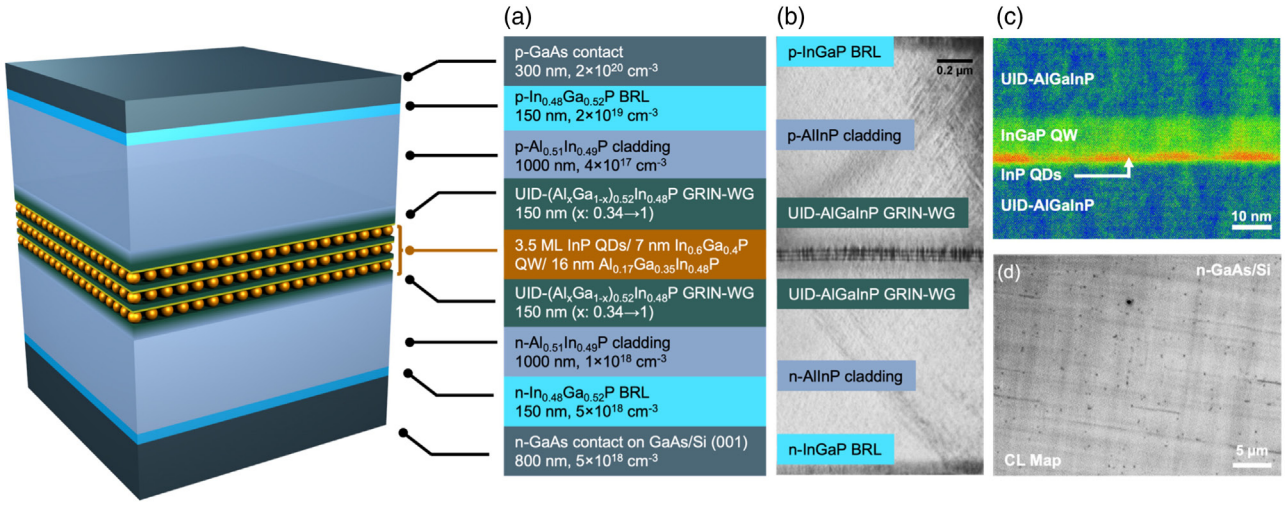

Fig. 1. (a) Growth schematic of InP MQD laser on GaAs/Si; the SQW laser is similar except without QDs and only one repeat of the active region; (b) BF-TEM image of InP MQD laser on GaAs/Si showing strain contrast around the InP QDs; (c) false-colored high-resolution HAADF-STEM image of a single InP QDWELL layer showing composition contrast from individual QDs; (d) CL map of n-GaAs/Si showing TDD of $\sim 1 \times 10^7$ cm^{-2} with dark spots correlating to threading dislocations.

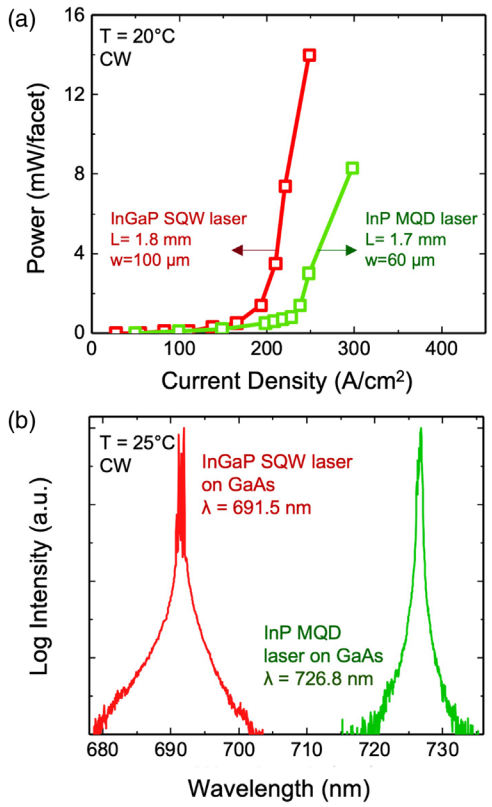

Fig. 2. Benchmark laser characteristics for devices grown on GaAs. (a) L-I curves for $In_{0.6}Ga_{0.4}P$ SQW (red, 1.8 mm cavity length with 100 μm ridge) and InP MQD (green, 1.7 mm cavity length with 60 μm ridge) lasers tested CW at 20°C, with $In_{0.6}Ga_{0.4}P$ SQW (InP MQD) laser exhibiting $J_{th} = 170$ A/cm^2 (230 A/cm^2); (b) semilogarithmic laser spectra showing $In_{0.6}Ga_{0.4}P$ SQW laser emitting at 691.5 nm and InP MQD laser emitting at 726.8 nm with multiple modes. The spectra were collected at RT under CW operation at $1.7 \times J_{th}$ for SQW lasers and $1.3 \times J_{th}$ for MQD lasers.

values observed by Kwon *et al.* on both GaAs and Si, which in turn dominates the effects of threading dislocations. For comparison, $In_{0.15}Ga_{0.85}As$ QW lasers on GaAs/Si with emission at ~1 μm and TDD $\sim 1 \times 10^8$ cm^{-2} exhibited pulsed J_{th} of 5.6 kA/cm^2, ~60× higher than their counterparts grown on GaAs (001) [37]. Our $In_{0.6}Ga_{0.4}P$ SQW lasers on Si appear to show a comparatively higher degree of tolerance to threading dislocations, which may result from the low carrier diffusivity in phosphides compared to arsenides [38]. In contrast, $Ga_xIn_{1-x}As_ySb_{1-y}$ QW lasers grown on GaSb on Si emitting at 2.3 μm with a TDD $= 1.4 \times 10^8$ cm^{-2} show only ~2× increase in J_{th} compared to lasers grown on GaSb [39]. Further study is needed to better understand the complex interplay of bandgap energy and composition on the dislocation tolerance of III-V lasers.

Figure 4(a) shows the RT, CW L-I characteristics of the first electrically injected InP MQD laser on GaAs/Si. J_{th} of this laser is 690 A/cm^2 (230 A/cm^2 per QDWELL layer), and the inset of Fig. 4(a) shows a photograph of the InP MQD laser (cavity length = 0.9 mm, ridge width = 40 μm) operating at ~5 mW output. The InP MQD laser on Si emits with multiple modes centered at 726.2 nm [Fig. 4(b)], nearly identical to our MQD lasers on GaAs. Unlike the slightly different wavelengths of the SQW lasers described above, here we attribute the lack of red-shift to minor differences in QD growth on GaAs versus GaAs/Si. In addition to differences in growth, the emission wavelength of QD lasers might be affected by differences in mirror loss due to the varying cavity lengths on GaAs and GaAs/Si. Figure 4(c) shows that J_{th} of the InP MQD laser on Si increases from 690 A/cm^2 at 20°C to 1063 A/cm^2 at 50°C. We extracted a characteristic temperature T_o of 65 K for InP MQD lasers on Si, which is lower than the value of 88 K for lasers on GaAs (Supplement 1). The lower T_o on Si indicates the need for improved heat dissipation in the active region and further reduction of TDD [40].

The InP MQD laser on GaAs/Si shows a J_{th} increase of 3× compared to its counterpart grown on GaAs, which is comparable to the 2× increase typically seen in InAs MQD lasers on Si [10]. Like QW lasers on Si, a part of the increase in J_{th} could be attributed to the shorter cavity length and narrower ridges. But based on previous PL studies where InP QDs showed similar intensity on both GaAs and GaAs/Si [29,35], we would have expected that the carrier confinement offered by the QDs would confer some J_{th} advantage for laser operation over the QWs. The high-level carrier

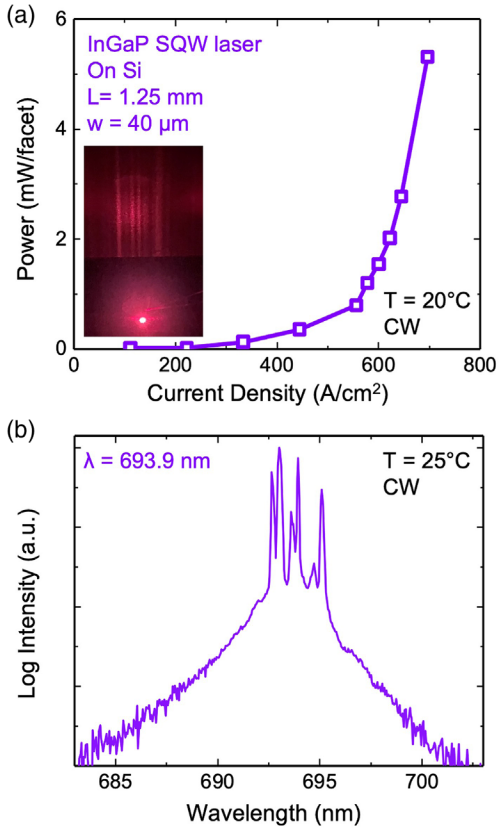

Fig. 3. (a) L-I curve for $In_{0.6}Ga_{0.4}P$ SQW laser on GaAs/Si (001) with a cavity length of 1.25 mm and ridge width of 40 μm operating CW at T = 20°C with J_{th} = 550 A/cm^2; inset, photograph of $In_{0.6}Ga_{0.4}P$ SQW laser on Si lasing with output power >5 mW projected on a wall ~50 cm away from device under test; (b) semilogarithmic lasing spectra of $In_{0.6}Ga_{0.4}$ P SQW laser on Si operating at 1.6 × J_{th}, collected at RT CW showing multiple mode emission centered at 693.9 nm.

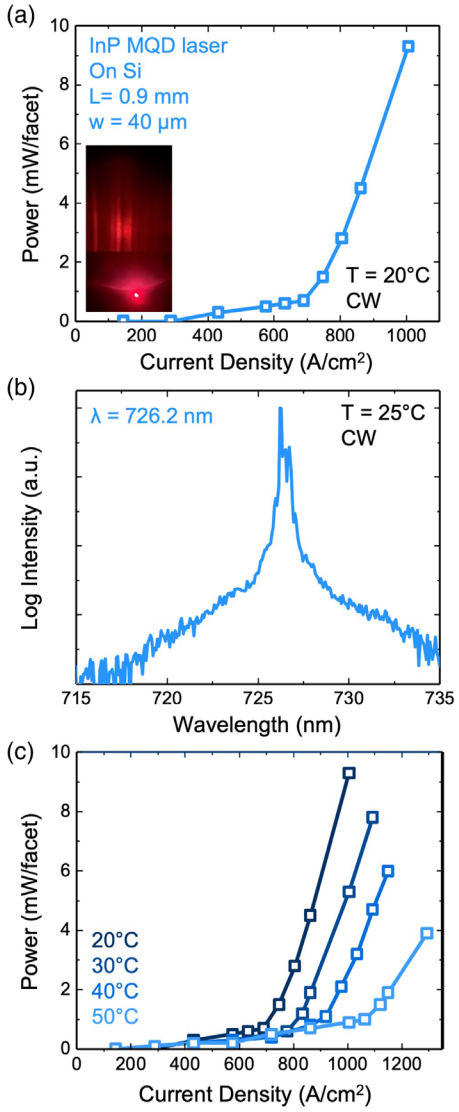

Fig. 4. (a) L-I curve for InP MQD laser on GaAs/Si (001) with a cavity length of 0.9 mm and ridge width of 40 μm operating CW at T = 20°C with J_{th} = 690 A/cm^2; inset, photograph of InP MQD laser on Si lasing with output power ~5 mW projected on a wall ~50 cm away from device under test; (b) semilogarithmic lasing spectra of InP MQD laser on Si operating at 1.1 × J_{th}, collected at RT under CW operation showing multiple mode emission centered in the far-red regime at 726.2 nm; (c) L-I curves for InP MQD laser on Si operating CW at elevated temperature of 20°C to 50°C showing an increase in J_{th} with characteristic temperature of 65 K.

injection inherent to laser operation may partly explain the qualitative discrepancy between the PL (taken at very low-level injection) and laser results. Future studies with optimized device design and processing could help further unveil the effects of threading dislocations on visible QW and QD lasers grown on Si.

Figure 5(a) shows that we achieved low-J_{th} operation for red and far-red lasers on both GaAs and GaAs/Si substrates. Despite a J_{th} increase of ~3× caused by threading dislocations, both $In_{0.6}Ga_{0.4}P$ SQW and InP MQD lasers on Si show comparable J_{th} to previously published red and far-red lasers grown on GaAs (Supplement 1). We believe that the use of a GRIN design for optical and electrical confinement, reduction of nonradiative recombination centers using RTA, and the inherent low diffusivity of carriers in phosphides are among the key factors for our low-J_{th} lasers on Si substrates. Figure 5(b) shows the spectra of $In_{0.6}Ga_{0.4}P$ SQW and InP MQD lasers on GaAs and Si spanning 680 to 730 nm. The emission wavelength range can be tailored to a wide range of applications by utilizing tensile-strained $In_xGa_{1-x}P$ QWs [41] for shorter wavelength and alloying InP QDs with arsenic for longer wavelength emission [42]. The performance of both the SQW and MQD lasers could be further improved by reducing the TDD of GaAs/Si virtual substrates [13] and exploring p-modulation doping in the QD active regions [43]. Future work will also aim to lower the threshold voltage of the devices by reduction of barriers to majority carriers and optimization of contact resistances [44]. For example, the $In_{0.6}Ga_{0.4}P$ SQW lasers on both GaAs and Si operate with a threshold voltage of 2.7 V, which is higher than expected for a laser emitting at a photon energy of ~1.8 eV; previously published lasers in this wavelength range operated at voltages of 2.1–2.3 V [33,45], indicating room for improvement. In addition to facet coating, we believe that lower J_{th} operation of $In_{0.6}Ga_{0.4}P$ QW and InP MQD lasers on Si can be achieved with systematic improvements in facet formation [18], as well as longer cavity lengths [33]. Future work will also aim toward testing the extrapolated operation lifetime of $In_{0.6}Ga_{0.4}P$ SQW and InP MQD lasers on Si and understanding their degradation mechanisms.

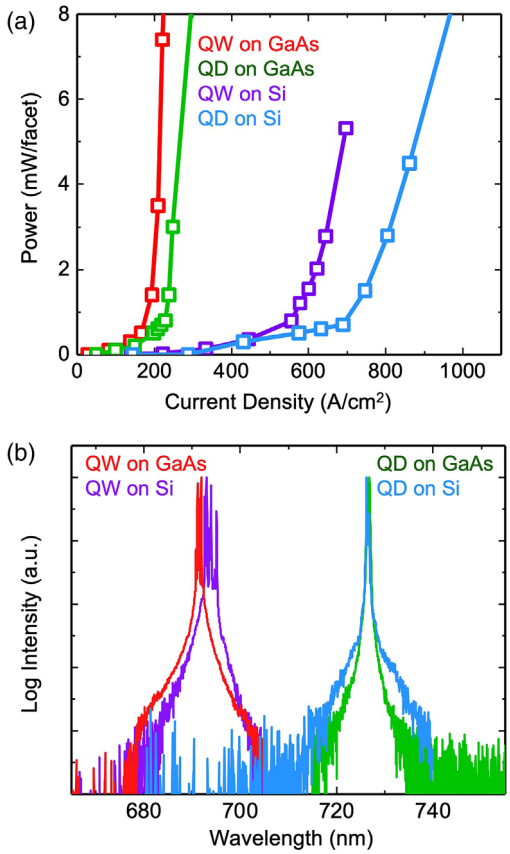

Fig. 5. (a) Comparison of L-I characteristics of $In_{0.6}Ga_{0.4}P$ SQW and InP MQD lasers on GaAs and GaAs/Si with both SQW and MQD lasers on Si showing a J_{th} increase of ~3× compared to lasers on GaAs; (b) spectra of $In_{0.6}Ga_{0.4}P$ SQW and InP MQD lasers grown on GaAs and GaAs/Si in semilogarithmic scale.

In conclusion, we demonstrated what we believe are the first RT, CW, electrically injected red $In_{0.6}Ga_{0.4}P$ SQW and far-red InP MQD lasers on Si (001) with respective J_{th} values of 550 A/cm^2 and 690 A/cm^2. This study indicates that the effect of dislocations on phosphide- and arsenide-based lasers on Si differ significantly, with arsenides showing stronger benefits in J_{th} by switching from a QW to a QD active region. III-V lasers based on diverse active region designs, compositions, and bandgap energies can all behave differently when grown on Si, and future studies will undoubtedly lead to deeper insights on these differences. Phosphide-based QW and QD lasers offer high performance over a wide range of wavelengths from 630 to 800 nm, and this work establishes that such lasers can be grown on Si (001). Combined with SiN_x waveguides, such short-wavelength lasers open the intriguing possibility of direct integration with highly sensitive Si photodetectors [46], circumventing the escalated dark current of epitaxial Ge/Si detectors [47]. Epitaxial QD and QW lasers emitting at 1.3–2.3 μm are becoming increasingly established, and this work takes a vital first step toward integration of red visible lasers that will allow integrated photonics to expand its impact into areas such as on-chip biosensing [48] and quantum computing [9].

Funding. Lincoln Laboratory, Massachusetts Institute of Technology; NASA Space Technology Research Fellowship (80NSSC18K1171, 80NSSC19K1174).

Acknowledgment. We thank Chris Heidelberger, Reuel Swint, and Paul Juodawlkis for helpful discussions and assistance. We also thank Katherine Lakomy and Prof. Kent Choquette for help with initial pulsed testing of the lasers.

We gratefully acknowledge funding from MIT Lincoln Laboratory under the program, "Heteroepitaxial III-V/SiN_x Integrated Photonics (HIP)". R. D. H and B. D. L were supported by NASA Space Technology Research Fellowships.

Disclosures. The authors declare no conflicts of interest.

Data availability. Data underlying the results presented in this paper are not publicly available at this time but may be obtained from the authors upon reasonable request.

Supplemental document. See Supplement 1 for supporting content.

REFERENCES

1. T. Pinguet, S. Denton, S. Gloeckner, M. Mack, G. Masini, A. Mekis, S. Pang, M. Peterson, S. Sahni, and P. D. Dobbelaere, "High-volume manufacturing platform for silicon photonics," Proc. IEEE **106**, 2281–2290 (2018).
2. G. Sanders, S. Sanders, L. Strandjord, T. Qiu, J. Wu, M. Smiciklas, D. Mead, S. Mosor, A. Arrizon, W. Ho, and M. Salit, "Fiber optic gyro development at Honeywell," Proc. SPIE **9852**, 985207 (2016).
3. M. Boerkamp, T. van Leest, J. Heldens, A. Leinse, M. Hoekman, R. Heideman, and J. Caro, "On-chip optical trapping and Raman spectroscopy using a TripleX dual-waveguide trap," Opt. Express **22**, 30528–30537 (2014).
4. J. Wang, F. Sciarrino, A. Laing, and M. G. Thompson, "Integrated photonic quantum technologies," Nat. Photonics **14**, 273–284 (2020).
5. K. D. Vos, I. Bartolozzi, E. Schacht, P. Bienstman, and R. Baets, "Silicon-on-insulator microring resonator for sensitive and label-free biosensing," Opt. Express **15**, 7610–7615 (2007).
6. A. D. Ludlow, M. M. Boyd, J. Ye, E. Peik, and P. O. Schmidt, "Optical atomic clocks," Rev. Mod. Phys. **87**, 637–701 (2015).
7. C. Sorace-Agaskar, S. Bramhavar, D. Kharas, W. Loh, P. Juodawlkis, J. Chiaverini, and J. Sage, "Multi-layer integrated photonics from the ultraviolet to the infrared," Proc. SPIE **10510**, 105100D (2018).
8. R. J. Niffenegger, J. Stuart, C. Sorace-Agaskar, D. Kharas, S. Bramhavar, C. D. Bruzewicz, W. Loh, R. T. Maxson, R. McConnell, D. Reens, G. N. West, J. M. Sage, and J. Chiaverini, "Integrated multi-wavelength control of an ion qubit," Nature **586**, 538–542 (2020).
9. D. J. Blumenthal, R. Heideman, D. Geuzebroek, A. Leinse, and C. Roeloffzen, "Silicon nitride in silicon photonics," Proc. IEEE **106**, 2209–2231 (2018).
10. A. Y. Liu, S. Srinivasan, J. Norman, A. C. Gossard, and J. E. Bowers, "Quantum dot lasers for silicon photonics [Invited]," Photon. Res. **3**, B1–B9 (2015).
11. S. Chen, W. Li, J. Wu, Q. Jiang, M. Tang, S. Shutts, S. N. Elliott, A. Sobiesierski, A. J. Seeds, I. Ross, P. M. Smowton, and H. Liu, "Electrically pumped continuous-wave III–V quantum dot lasers on silicon," Nat. Photonics **10**, 307–311 (2016).
12. D. Jung, J. Norman, M. J. Kennedy, C. Shang, B. Shin, Y. Wan, A. C. Gossard, and J. E. Bowers, "High efficiency low threshold current 1.3 μm InAs quantum dot lasers on on-axis (001) GaP/Si," Appl. Phys. Lett. **111**, 122107 (2017).
13. C. Shang, E. Hughes, Y. Wan, M. Dumont, R. Koscica, J. Selvidge, R. Herrick, A. C. Gossard, K. Mukherjee, and J. E. Bowers, "High-temperature reliable quantum-dot lasers on Si with misfit and threading dislocation filters," Optica **8**, 749–754 (2021).
14. Y. Wan, C. Shang, J. Norman, B. Shi, Q. Li, N. Collins, M. Dumont, K. M. Lau, A. C. Gossard, and J. E. Bowers, "Low threshold quantum dot lasers directly grown on unpatterned quasi-nominal (001) Si," IEEE J. Sel. Top. Quantum Electron. **26**, 1–9 (2020).
15. B. Shi, H. Zhao, L. Wang, B. Song, S. T. Suran Brunelli, and J. Klamkin, "Continuous-wave electrically pumped 1550 nm lasers epitaxially grown on on-axis (001) silicon," Optica **6**, 1507–1514 (2019).
16. B. Shi, S. Pinna, H. Zhao, S. Zhu, and J. Klamkin, "Lasing characteristics and reliability of 1550 nm laser diodes monolithically grown on silicon," Phys. Status Solidi A **218**, 2000374 (2021).
17. M. Rio Calvo, L. Monge Bartolomé, M. Bahriz, G. Boissier, L. Cerutti, J.-B. Rodriguez, and E. Tournié, "Mid-infrared laser diodes epitaxially grown on on-axis (001) silicon," Optica **7**, 263–266 (2020).
18. J. R. Reboul, L. Cerutti, J. B. Rodriguez, P. Grech, and E. Tournié, "Continuous-wave operation above room temperature of GaSb-based laser diodes grown on Si," Appl. Phys. Lett. **99**, 121113 (2011).

19. S. Pan, V. Cao, M. Liao, Y. Lu, Z. Liu, M. Tang, S. Chen, A. Seeds, and H. Liu, "Recent progress in epitaxial growth of III–V quantum-dot lasers on silicon substrate," J. Semicond. **40**, 101302 (2019).
20. C. Shang, Y. Wan, J. Selvidge, E. Hughes, R. Herrick, K. Mukherjee, J. Duan, F. Grillot, W. W. Chow, and J. E. Bowers, "Perspectives on advances in quantum dot lasers and integration with Si photonic integrated circuits," ACS Photon. **8**, 2555–2566 (2021).
21. Y. Sun, K. Zhou, M. Feng, Z. Li, Y. Zhou, Q. Sun, J. Liu, L. Zhang, D. Li, X. Sun, D. Li, S. Zhang, M. Ikeda, and H. Yang, "Room-temperature continuous-wave electrically pumped InGaN/GaN quantum well blue laser diode directly grown on Si," Light Sci. Appl. **7**, 13 (2018).
22. H. Nguyen-Van, A. N. Baranov, Z. Loghmari, L. Cerutti, J.-B. Rodriguez, J. Tournet, G. Narcy, G. Boissier, G. Patriarche, M. Bahriz, E. Tournié, and R. Teissier, "Quantum cascade lasers grown on silicon," Sci. Rep. **8**, 7206 (2018).
23. G. M. Lewis, J. Lutti, P. M. Smowton, P. Blood, A. B. Krysa, and S. L. Liew, "Optical properties of InP/GaInP quantum-dot laser structures," Appl. Phys. Lett. **85**, 1904–1906 (2004).
24. J. Lutti, P. M. Smowton, G. M. Lewis, A. B. Krysa, J. S. Roberts, P. A. Houston, Y. C. Xin, Y. Li, and L. F. Lester, "740 nm InP/GaInP quantum-dot laser with 190 A cm^{-2} room temperature threshold current density," Electron. Lett. **41**, 247–248 (2005).
25. S. Shutts, P. M. Smowton, and A. B. Krysa, "Dual-wavelength InP quantum dot lasers," Appl. Phys. Lett. **104**, 241106 (2014).
26. L. Z. Wu and Y. S. Zhang, "Selenium doping effects and low-threshold high-power GaInP-AlGaInP single-quantum-well lasers grown by MOVPE," IEEE Photon. Technol. Lett. **12**, 248–250 (2000).
27. P. Savolainen, M. Toivonen, J. Kongas, M. Pessa, P. Corvini, and M. Jansen, "Record quantum efficiency (92%) operation of 680 nm GaInP/AlGaInP ridge waveguide singlemode lasers," Electron. Lett. **34**, 1104–1105 (1998).
28. O. Kwon, J. J. Boeckl, M. L. Lee, A. J. Pitera, E. A. Fitzgerald, and S. A. Ringel, "Monolithic integration of AlGaInP laser diodes on SiGe/Si substrates by molecular beam epitaxy," J. Appl. Phys. **100**, 013103 (2006).
29. W. Luo, L. Lin, J. Huang, Y. Han, and K. M. Lau, "Red-emitting InP quantum dot micro-disk lasers epitaxially grown on (001) silicon," Opt. Lett. **46**, 4514–4517 (2021).
30. C. Martinez, V. Krotov, B. Meynard, and D. Fowler, "See-through holographic retinal projection display concept," Optica **5**, 1200–1209 (2018).
31. D. Jung, P. G. Callahan, B. Shin, K. Mukherjee, A. C. Gossard, and J. E. Bowers, "Low threading dislocation density GaAs growth on on-axis GaP/Si (001)," J. Appl. Phys. **122**, 225703 (2017).
32. K. Itaya, M. Ishikawa, Y. Watanabe, K. Nitta, G.-I. Hatakoshi, and Y. Uematsu, "A new transverse-mode stabilized InGaAlP visible light laser diode using p-p isotype heterobarrier blocking," Jpn. J. Appl. Phys. **27**, L2414–L2416 (1988).
33. M. Jalonen, M. Toivonen, P. Savolainen, J. Köngäs, and M. Pessa, "Effects of rapid thermal annealing on GaInP/AlGaInP lasers grown by all-solid-source molecular beam epitaxy," Appl. Phys. Lett. **71**, 479–481 (1997).
34. S. Tomasulo, J. Simon, P. J. Simmonds, J. Biagiotti, and M. L. Lee, "Molecular beam epitaxy of metamorphic $In_yGa_{1-y}P$ solar cells on mixed anion $GaAs_xP_{1-x}$/GaAs graded buffers," J. Vac. Sci. Technol. B **29**, 03C118 (2011).
35. P. Dhingra, S. Fan, Y. Sun, R. D. Hool, B. Eng, and M. L. Lee, "InP quantum dots for dislocation-tolerant, visible light emitters on Si," Appl. Phys. Lett. **117**, 181102 (2020).
36. Y. Sun, S. Fan, J. Faucher, R. D. Hool, B. D. Li, P. Dhingra, and M. L. Lee, "2.0–2.2 eV AlGaInP solar cells grown by molecular beam epitaxy," Sol. Energy Mater. Sol. Cells **219**, 110774 (2021).
37. X. Huang, Y. Song, T. Masuda, D. Jung, and M. Lee, "InGaAs/GaAs quantum well lasers grown on exact GaP/Si (001)," Electron. Lett. **50**, 1226–1227 (2014).
38. N. Jain and M. K. Hudait, "Impact of threading dislocations on the design of GaAs and InGaP/GaAs solar cells on Si using finite element analysis," IEEE J. Photovolt. **3**, 528–534 (2013).
39. L. Monge-Bartolome, B. Shi, B. Lai, G. Boissier, L. Cerutti, J.-B. Rodriguez, K. M. Lau, and E. Tournié, "GaSb-based laser diodes grown on MOCVD GaAs-on-Si templates," Opt. Express **29**, 11268–11276 (2021).
40. J. Kwoen, B. Jang, K. Watanabe, and Y. Arakawa, "High-temperature continuous-wave operation of directly grown InAs/GaAs quantum dot lasers on on-axis Si (001)," Opt. Express **27**, 2681–2688 (2019).
41. P. M. Smowton, G. M. Lewis, P. Blood, and W. W. Chow, "Optimization of 635-nm tensile strained GaInP laser diodes," IEEE J. Sel. Top. Quantum Electron. **9**, 1246–1251 (2003).
42. I. Karomi, P. M. Smowton, S. Shutts, A. B. Krysa, and R. Beanland, "InAsP quantum dot lasers grown by MOVPE," Opt. Express **23**, 27282–27291 (2015).
43. J. C. Norman, Z. Zhang, D. Jung, C. Shang, M. Kennedy, M. Dumont, R. W. Herrick, A. C. Gossard, and J. E. Bowers, "The importance of p-doping for quantum dot laser on silicon performance," IEEE J. Quantum Electron. **55**, 1–11 (2019).
44. J. Piprek, "What limits the efficiency of high-power InGaN/GaN lasers?" IEEE J. Quantum Electron. **53**, 1–4 (2017).
45. P. Savolainen and M. Pessa, "High-power, high-efficiency GaInP/AlGaInP laser diode," Jpn. J. Appl. Phys. **35**, L1501–L1502 (1996).
46. A. H. Atabaki, S. Moazeni, F. Pavanello, H. Gevorgyan, J. Notaros, L. Alloatti, M. T. Wade, C. Sun, S. A. Kruger, H. Meng, K. Al Qubaisi, I. Wang, B. Zhang, A. Khilo, C. V. Baiocco, M. A. Popović, V. M. Stojanović, and R. J. Ram, "Integrating photonics with silicon nanoelectronics for the next generation of systems on a chip," Nature **556**, 349–354 (2018).
47. J. Michel, J. Liu, and L. C. Kimerling, "High-performance Ge-on-Si photodetectors," Nat. Photonics **4**, 527–534 (2010).
48. D. Kohler, G. Schindler, L. Hahn, J. Milvich, A. Hofmann, K. Länge, W. Freude, and C. Koos, "Biophotonic sensors with integrated Si_3N_4-organic hybrid (SiNOH) lasers for point-of-care diagnostics," Light Sci. Appl. **10**, 64 (2021).